University of British Columbia - Okanagan

Kelowna BC, Canada

PHYS 331 Term 1 2023W

December 2023

Determining the Gravitational Constant Through Automation of a Classical Experiment

Skyler Alderson

Abstract

Using a torsion balance with a mirror, a laser, and a linear array of phototransistor, the gravitational constant G was measured. The mirror reflected the laser, allowing the oscillations of the torsion balance to be characterized by observing the instantaneous angle of the torsion pendulum using the phototransistor array. A pair of heavy masses were placed near the torsion balance; by shifting the position of these heavy masses, the shift in the equilibrium position of the oscillations could be used to extract G. This experiment found that $G = (5.5 \pm 0.6) \times 10^{-11}$ $\mathrm{m^3 kg^{-1} s^{-2}}$.

1 History and Motivation

Henry Cavendish first performed his iconic Cavendish experiment around 1798 to calculate the gravitational constant G used in Newton's famous gravitational force equation [1]. This constant would help quantify the movement of celestial bodies through the sky as it is the constant of proportionality between the ratio of the product of masses over the square of the distance to the force between the bodies. Scientist at the time had long been seeking out alternatives to describing the strength of gravity, such as the Schiehallion experiment in 1774 which sought to find the density of earth which could ultimately be used for an alternative approach to find G [2].

Cavendish's original experiment found the gravitational constant to be $G = 6.74 \times 10^{-11}$ $\mathrm{m^3 kg^{-1} s^{-2}}$, which is within 1% of the modern accepted value [1]. This experiment has been repeated many times since by many scientist and has become a standard experiment to try and determine the gravitational constant [3]. It is continued to be used in the 21st century to make accurate measurements of the gravitational constant with very little modifications to the apparatus itself.

The gravitational constant is notoriously difficult to measure precisely. Unlike many other fundamental constants which is known to a value of within few parts per billion, the gravitational constant is only known to a relative uncertainty of 10^{-5} [4]. Despite this, the Cavendish still proves to be a useful experiment in the modern day thanks to its fame and simple apparatus, allowing it to be a useful tool for demonstrative purposes.

2 Experimental Apparatus

The apparatus can be divided into three parts: the torsion balance atop an isolating stand, a laser, and a detector array. Fig. 1 shows the torsion balance, which remains quite similar in principle to the one used by Cavendish, simply updated to a modern design for ease of use and precision. The torsion balance suspends a horizontal rod (the torsion pendulum) from a long thin piece of string (the torsion ribbon). On both ends of the torsion pendulum sits a small metal sphere with a radius of $r = 7.56 \pm 0.05$ mm. These metal spheres sit at a distance away from the centre of the pendulum $d = 49.9 \pm 0.5$ mm. Attached to the centre of the pendulum is a mirror that reflects the laser, which can be used to determine the angle of the pendulum.

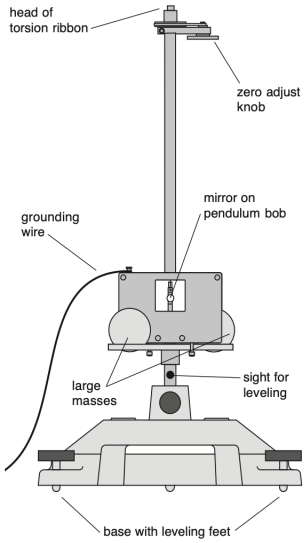

Figure 1: The exterior view of the side of a torsion view. Not visible is the horizontal rod of the torsion balance, which holds the centres of the small metal spheres level with the centres of the large metal spheres [5].

Attached to the torsion balance is a swivel support used to hold two large lead spheres, each with mass $M = 1500 \pm 1$ g. This swivel support holds the metals spheres such that they are close to the small metal spheres and thus their exerted gravitational force is non-negligible. The swivel support can be placed in one of two positions for the experiment, where these two positions are a reflection about the axis of the pendulum (or equivalently reflected about the axis through the mirror), such as is seen in Fig. 2. In both configurations, the distance between the centre of a large sphere to the centre of the closest small sphere was $b = 46.5 \pm 0.1$ mm.

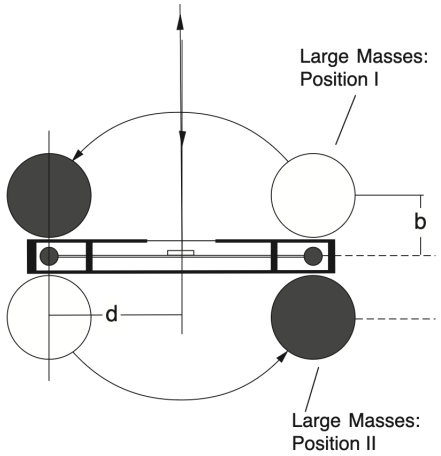

Figure 2: A top-down view of the torsion balance, showing position one and two of the large metal spheres. The small metal spheres are held at a height such that their centre of mass is at the same height as the centre of mass of the large spheres [5].

The array of 80 phototransistor are placed at a distance of $L = 242.5 \pm 0.5$ cm away from the torsion balance. Each phototransistor is spaced by a distance of $d_p = 5$ mm. When the laser illuminates one of the phototransistors, the known positions of the phototransistors are used to record the angle of the pendulum. This data is used to plot the amplitude of oscillation over time.

The torsion balance is situated on a pedestal that is held down by sandbags and sits atop four springy balls. This is done to minimise the impact of external vibrations affecting the apparatus. An accelerometer is attached to the pedestal to measure the amplitude of such external forces. The accelerometer is connected to HI-pass filters to remove the constant gravitational force before connecting to an analogue-digital converter so it can be automatically recorded.

3 Theory

3.1 Using the Torsion Balance to Measure G

Following the derivation by J. Andrews and J. Bobowski, if θ is the angular displacement from the equilibrium position, the drag torque is assumed to be proportional to $\dot{\theta}$, and κ is a constant to describe restoring force, then the moment of inertia I can be described by

$$I\dot{\theta} = 2\frac{GMm}{b^2}d - \frac{2I}{\tau}\dot{\theta} - \kappa\theta \tag{1}$$

where τ is the damping time constant [**6**]. The first term in this equation describes the contribution by gravitational force, the second term is the drag force, and the third is the restoring torque caused by the ribbon. It is assumed that b, the distance between the large and small lead spheres, remains approximately constant during the oscillations. The equilibrium state of $\ddot{\theta} = \dot{\theta} = 0$ gives

$$\theta_0 = \frac{2}{\kappa}\frac{GMm}{b^2}d. \tag{2}$$

In the case where the oscillations are under-damped with a resonant frequency of ω_0 where $\omega_1^2 = \omega_0^2 - \tau^{-2}$, Eq. (2) allows Eq. (1) to be rewritten as

$$G = \frac{\Delta\theta_0 b^2 I}{4Mmd}\left(\omega_1^2 + \frac{1}{\tau^2}\right), \tag{3}$$

after noticing that $\Delta\theta_0 = 2\theta_0$ since when the large spheres are placed in their second configuration, their equilibrium angle is $-\theta_0$. Since the angle of oscillations is very small, $\Delta S/2$ is a good approximation for the arclength $L\Delta\theta_0$, where S is the equilibrium position of the laser and hence ΔS is the chance in equilibrium position between the two configurations of the large masses. Finally, by the parallel axis theorem allows Eq. (3) to be expressed as

$$G = \frac{\Delta S b^2}{4MdL}\left(d^2 + \frac{2}{5}r^2\right)\left(\omega_1^2 + \frac{1}{\tau^2}\right). \tag{4}$$

All of the quantities in Eq. (4) are measurable from the apparatus or the trials.

3.2 Parameterisation and Curve Fitting

The curve traced out on the phototransistor array by the reflected laser is a decaying sinusoidal wave and thus can be described by

$$y = Ae^{-\frac{t-t_0}{\tau}}\sin\left[\omega_1(t-t_0)+\phi\right] + S, \tag{5}$$

where A is the amplitude of the oscillation, ϕ is the initial phase, t_0 is the time-offset, and t is time. A curve-fit can be used to extract ω_1, τ, and ΔS where these are used to find G through Eq. 4.

When performing a non-linear curve-fit, unnecessary variables will introduce vary large errors due to there being too many degrees of freedom. The curve-fitting function will be able to find multiple values for these extra parameters that will satisfy the curve and thus is cannot determine their exact value. In other words, if the function is over-parameterised, then the errors associated with the curve-fit will be large.

In order to perform a fit that will result in low errors, extra parameters have to be eliminated. By ensuring that our initial phase is zero, we can remove ϕ. Similarly, if our curve begins at a time of zero, then t_0 can be eliminated.

$$y = Ae^{-\frac{t}{\tau}}\sin\left(\omega_1 t\right) + S. \tag{6}$$

Fig. 3 shows an over-parameterised trial and Fig. 4 shows the same data but adjusted such that it is not over-parameterised and thus can be described by Eq. 6.

While additional parameters could be eliminated, such as removing A by normalising the amplitude, eliminating additional parameters introduces bias. After having removed t_0 and ϕ, the fit function is no longer over-parameterised.

To determine whether the function is over-parameterised, the diagonal elements of the matrix returned by the curve-fit can be checked. If any elements of the diagonal are much larger than one, then they are unnecessary. A curve-fit performed on Eq. 5 returned two elements of the diagonal, corresponding to t_0 and ϕ, that were many orders of magnitude larger than one. A curve-fit on Eq. 6 returned values comparable to one.

3.3 Automation of Data Collection

When the apparatus' laser illuminates a phototransistor, it allows current to flow through it and thus produce a HI signal. Otherwise, when the phototransistor is not illuminated, it reads LO. The state of the phototransistors is serially checked by a counting circuit and multiplexers (MUXs). The positive edge of each clock cycle the circuit is used to poll the state of the next phototransistor as determined by the MUXs. The negative edge of the clock would increment the address on the MUXs to the next phototransistor. A data-acquisition device (DAQ) is used to collect the HI outputs of the MUXs and record it to a program called LabView; on a LO output, no data is collected.

The multiplexers have 16 inputs and so five are needed in order to address the 80 phototransistors. Each MUX is directly mapped to a consecutive batch of 16 phototransistors. Two counters are used, one 16-cycle

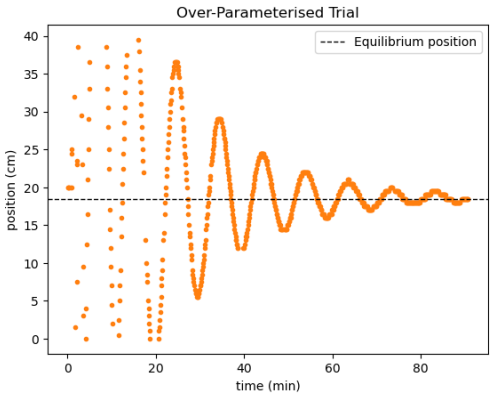

Figure 3: The raw data from an example trial. This corresponds to a decaying sin wave with some time-offset and a non-zero phase.

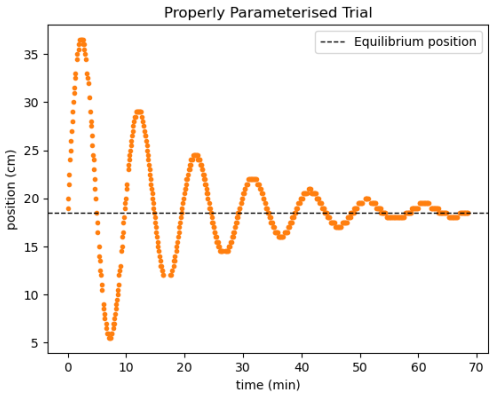

Figure 4: The same data from Fig. 3 that has been processed to remove unnecessary parameters. This corresponds to a decaying sinusoidal wave with a time-offset of zero and a phase of zero.

counter and a one 5-cycle counter. The 16-cycle counter polls the state of the 16 phototransistors addressed by each of the five MUXs simultaneously before incriminating the MUXs' addresses. The output of these five MUXs are passed onto a final MUX, to which the 5-cycle counter connects. This final MUX selects which of the previous five MUXs' outputs are passed to the DAQ. The 5-cycle counter increments after the 16-cycle counter completes a full period and resets to zero.

4 Experimental Methods

4.1 Data Trials

The laser was centred such that its beam reflected off of the torsion balance's mirror and could be detected by the phototransistor array without the amplitude of the oscillation being so great as for the beam to sweep beyond the array. We had the reflected beam hit the array off to one side such that when we shifted the large masses, the beam would continue to remain within the phototransistor array's breadth despite oscillating about a new equilibrium position.

To begin collecting data, we started the data collection program before we brought a small magnet near the small masses. When the restoring force on the torsion balance was in equilibrium with the magnetic force on the sphere, the magnet was quickly removed. This caused the torsion pendulum to begin oscillating. After approximately an hour and a half, the oscillations had decayed to less than the distance between two consecutive phototransistors, and thus too small for us to measure. At that point, we began the second trial by shifting the large masses to their second position before using the magnet to begin the oscillations again. The data collection continue between trials since we wanted several trials on the same recording to facilitate the comparison between equilibrium positions. For the third trial, after the oscillations of the second trial had become negligible, we returned the masses to their original position and began the oscillations anew. While it is only necessary to perform two trials, the third trial was performed to ensure that the equilibrium position was the same between the first and third trial, that it had not shifted as a result of adjusting the apparatus.

When the third trial was concluded, the data was analysed using Python. Non-linear fits were performed on subsections of the output data corresponding to each trial.

4.2 Isolation Trials

To ensure the system was isolated from the surroundings, additional trials were performed. External vibrations would affect the oscillation of the torsion balance. Even if the magnitude of these vibrations are small,

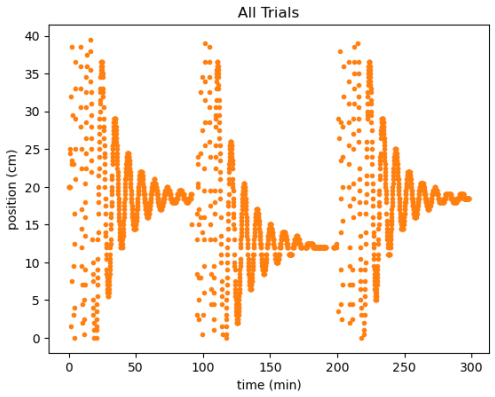

Figure 5: Three trials of the torsion balance. The first and third trial have the same equilibrium position that is offset from the equilibrium position of trial two.

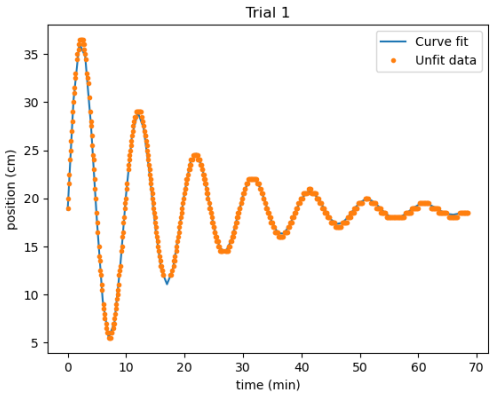

Figure 6: The first trial plotted on a section where it is not over-parameterised. It has been plotted alongside the trial's best-fit function.

the the gravitational force itself is extremely weak and thus disturbances to the system can significantly affect the measurements. The isolation trials did not use the torsion balance but rather an accelerometer attached to the pedestal. To perform these trials, the data collection program was started. No other setup was necessary, other than very quietly stepping out of the room. These trials ran for 90 minutes. This duration was selected as it would be able to sample at least one period of usual activity within the building, and thus the vibrations caused by work elsewhere in the building. When finished, the program had recorded the magnitude of acceleration in all three axes both as a function of time and as a function of frequency.

Two of these trials were performed. The first trial had the same setup as was performed in the experiment: the pedestal was held down by sandbags and sat atop springy balls; this acted as a damped oscillator to minimise the effect of external vibrations. The second trial removed the weights and springs such that the pedestal was resting directly on the ground. These two trails were performed to ensure that steps taken to isolate the pedestal indeed ensured the building's vibrations did not affect the oscillation of the pendulum.

5 Results

5.1 Findings

To obtain w_1, τ, the mean value between the three trials were used. ΔS was taken to the average between both shifts in position, that is the average of $S_1 - S_2$ and $S_3 - S_2$ where S_i is the equilibrium position from the ith trial. Propagation of errors was used to determine the uncertainty on G.

Fig. 5 shows all trials and Fig. 6 show the first trial with the fit curve. The three trials have a mean angular frequency of $\omega_1 = (1.070 \pm 0.0002) \times 10^{-2}$ s^{-1} and a mean damping time constant of $\tau = 1074 \pm 4$ s^{-1}. The change in equilibrium position between the trials is $\Delta S = 6.4 \pm 0.3$ cm. These values give us a value for the gravitational constant: $G = (5.5 \pm 0.6) \times 10^{-11}$ m^{3}kg^{-1}s^{-2}. This value of G is not within uncertainty of the accepted value.

In Fig. 5, each trial begins with erratic data. This is due to the the laser sweeping across the phototransistor array faster than the automatic data collection circuit can poll every phototransistor. As a result, the laser appears to skip over phototransistors. Furthermore, the pendulum of the torsion balance had sufficient angular velocity to hit the casing. Both of these cause the initial 30 minutes of each trial to be unreliable; our fits are performed when the data becomes reliable. Both problems were both caused by too great of an initial angular velocity of the torsion pendulum and both issues disappeared when the pendulum slows.

The initial erratic behaviour of the curves have little effect on the results. Neither the equilibrium position nor the time decay constant would be greatly affected by initial behaviour. In having to remove the initial data for our fits, the uncertainties of these variables have been increased since our fit will be performed using

a smaller amount of data. However, there is still more than enough data to perform a reasonable curve-fit after the data had been trimmed.

In all trials, the curve traced out by the laser does not go below zero centimetres. Because the position of the reflected laser was measured by an array of phototransistors, a position prior to the first phototransistor could not be measure. A position less than zero centimetres would correspond to the laser sweeping beyond the edge of the phototransistor array. Since the reflected laser is out of range only during portions of each trial where the data is discarded anyways, this does not affect the results anymore than the initial erratic behaviour.

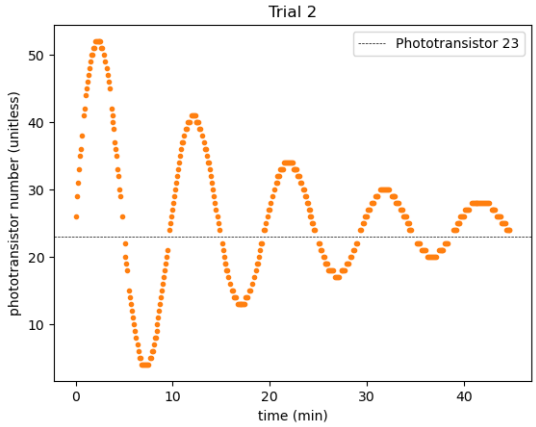

Figure 7: The second trial of the torsion balance. A horizontal line is drawn at the 23rd phototransistor to show that it is never illuminated.

On the phototransistor array, phototransistor 23 did not respond to the laser. Fig. 7 shows this clearly, where a horizontal line can be placed at the 23rd phototransistor without intersecting any data points despite bisecting the curve. While there are previous missing data points, those occur when the laser has a greater angular velocity than the polling speed of the automatic data collection circuit. Since phototransistor 23 always outputs a LO signal throughout all trials, even during times when the laser's angular velocity is small, the cause is a fault somewhere in the data collection apparatus. This fault is visible on all trials, but most prevalent during trial two. The issue may lie in a dead phototransistor or a loose connection within the data collection circuit.

A single faulty phototransistor negligibly affects the findings. The loss of a single phototransistor does not prevent the shape of the curve from being clearly resolved, thus the curve-fit would continue to produce fits with small errors. Even if the phototransistor corresponded to the equilibrium position, the best-fit parameters would not be significantly affected.

5.2 Mechanical Isolation

Figures 8, 10, and 12 show the undamped data from the accelerometer next to the damped data in figures 9, 11, and 13. In the undamped trials, a clear peak is seen in both the x- and y-directions at a frequency of 18 Hz; this peak disappears in the damped trials. These larges peaks have an approximate peak acceleration of 1×10^{-4} ms^{-2}. All trials have a mean magnitude of acceleration near 4×10^{-6} ms^{-2}; the damping does not improve the mean magnitude of acceleration.

In all isolation trials, there were thin peaks whose range of amplitudes were about one order of magnitude larger than the mean magnitude of acceleration. This is significantly less than the height of the wide peaks. Unlike the large peaks visible in the undamped trials, these peaks appear to have a negligible width. While the wide peaks correspond to the resonant frequency of the building, the thin peaks likely were caused by single spontaneous actions, such as a nearby door being closed, rather than resonant vibrations. Additional evidence to support this claim would be that these thin peaks are significantly more prominent in the y-direction than the x-direction, which is consistent to these spontaneous actions being oriented in the same axis as the sensor.

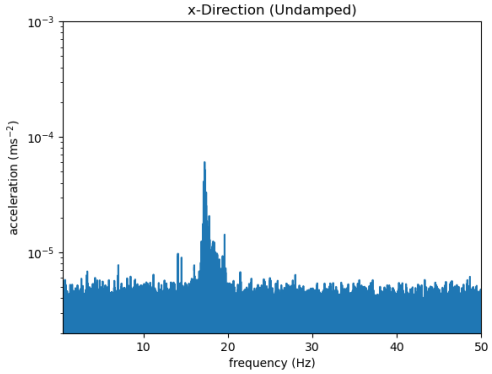

Figure 8: The undamped acceleration in the x-direction. A prominent peak is centred around 18 Hz.

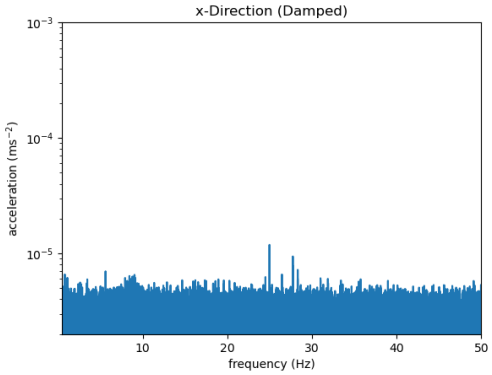

Figure 9: The damped acceleration in the x-direction.

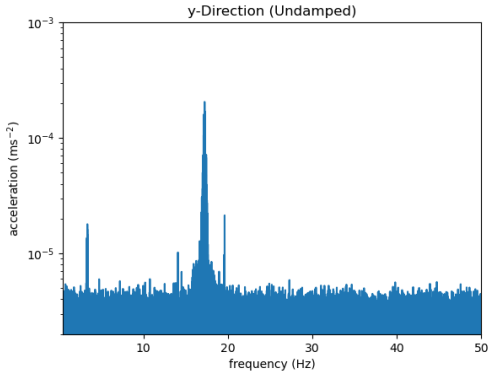

Figure 10: The undamped acceleration in the y-direction. A prominent peak is centred around 18 Hz.

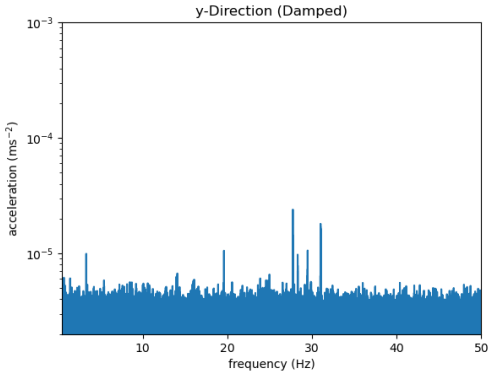

Figure 11: The damped acceleration in the y-direction.

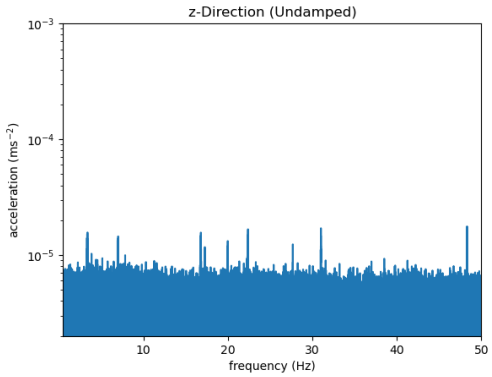

Figure 12: The undamped acceleration in the z-direction.

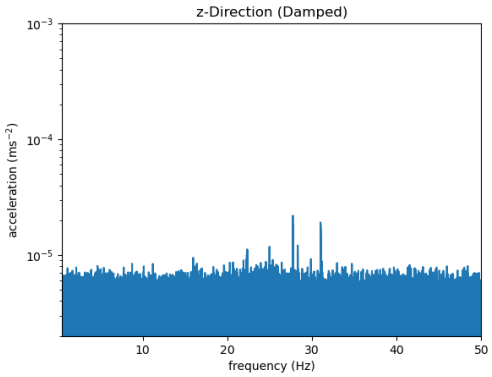

Figure 13: The damped acceleration in the z-direction.

The thin peaks share some similarities between Fig. 10 and Fig. 11, the undamped and damped trials in the y-direction. Both trials exhibit a peak near 4 Hz and another at 20 Hz. In the undamped trial, these peaks are approximately twice as tall as the damped trial. A dissimilarity between the trials is that there are a series of thin peaks scattered near 30 Hz in the damped trials whose max acceleration is similar to the thin peaks in the undamped trial. These may have been introduce by the mechanism used to isolate the torsion balance or, more likely, were caused some some external action that did not occur during the undamped trial. If the peaks were introduced by the isolation mechanism, then the peaks would have a greater thickness corresponding to a range of frequencies caused by the damping.

While the accelerometer gathered data for the z-direction (vertical to the pedestal), the results proved not to be elucidating. In the undamped trial, there was no wide peak; hence, the damped trial appears to be within random variations from the undamped trial. While thin peaks are present in both trials, no statistical significance could be concluded excluding the peaks clustered near 30 Hz.

The isolation mechanism was successful in decoupling the torsion balance's pedestal from the resonant frequency of the building, however it was insufficient in isolating it from all external vibrations. Additional steps would have improved the accuracy of the experiment, such as placing the apparatus further away from human activity.

6 Conclusion

This experiment was able to measure a value for the gravitational constant, $G = (5.5 \pm 0.6) \times 10^{-11}$ $\mathrm{m^3 kg^{-1} s^{-2}}$; however, the determined value did not lie within uncertainty of the accepted value. While the steps taken to isolate the apparatus from external vibrations successfully decoupled it from the building's resonant frequency, it failed to fully isolate the torsion balance from nearby spontaneous human activity. Additionally, the laser and phototransistor array were not isolated. External vibrations would affect these pieces of equipment less, due to them not performing experiment-critical delicate oscillation, nevertheless it may have introduced faulty readings when the vibrations shifted the position of the laser.

Further sources of error include initial angular frequencies that were too great. This led to the reflected laser sweeping faster than it can reliably be detected through the automatic data collection apparatus, the torsion pendulum slamming into its casings at the extreme angles during the initial oscillations, and the laser sweeping beyond the edge of the sensors. These issues were resolved by discarding data during the first 30 minutes of each trial, but such a step reduces the precision of the curve-fit used to extract parameters crucial for the calculation of G. Moreover, the lack of granularity caused by the discrete sensors with non-negligible distances between them reduces the clarity of the curve, which was compounded by the failure in one of the phototransistors for the duration of the experiment. These sources of errors led to ΔS, obtained through curve-fitting, contributing the greatest amount of error to the results; it had a relative uncertainty of 5% whereas other measurements were between 1% and 0.1% of relative uncertainty.

References

[1]H. Cavendish, *Xxi. experiments to determine the density of the earth* (The Royal Society, Dec. 1798), pp. 469–526.

[2]N. Maskelyne, *Xlix. an account of observations made on the mountain schehallien for finding its attraction* (The Royal Society, 1175), pp. 500–542.

[3]A. Mann, "The curious case of the gravitational constant", Proceedings of the National Academy of Sciences **113**, 9949–52 (Sept. 2016).

[4]C. Rothleitner and S. Schlamminger, "Invited review article: measurements of the newtonian constant of gravitation, g", Review of Scientific Instruments, `10.1063/1.4994619` (Nov. 2017).

[5]"Instruction manual and experiment guide for the pasco scientific model ap-8215 gravitational torsion balance", PASCO Scientific.